To appear in the *Astrophysical Journal*
Preprint typeset using LaTeX style emulateapj v. 5/2/11

arXiv:1401.7346v1 [astro-ph.SR] 28 Jan 2014

A 33 YEAR CONSTANCY OF THE X-RAY CORONAE OF AR LAC AND ECLIPSE DIAGNOSIS OF SCALE HEIGHT

Jeremy J. Drake,[1] Peter Ratzlaff,[1] Vinay Kashyap,[1] David P. Huenemoerder,[2] Bradford J. Wargelin,[1] Deron O. Pease[3]
[1]Harvard-Smithsonian Center for Astrophysics,
60 Garden Street, Cambridge, MA 02138
[2]Massachusetts Institute of Technology, Kavli Institute for Astrophysics and Space Research,
77 Massachusetts Avenue, Cambridge, MA 02139 and
[3]University of California, Berkeley, Space Sciences Laboratory,
7 Gauss Way,Berkeley, CA 94720
To appear in the Astrophysical Journal

ABSTRACT

Extensive X-ray and extreme ultraviolet (EUV) photometric observations of the eclipsing RS CVn system AR Lac were obtained over the years 1997 to 2013 with the *Chandra X-ray Observatory* *Extreme Ultraviolet Explorer*. During primary eclipse, HRC count rates decrease by ∼40%. A similar minimum is seen during one primary eclipse observed by *EUVE* but not in others owing to intrinsic source variability. Little evidence for secondary eclipses is present in either the X-ray or EUV data, reminiscent of earlier X-ray and EUV observations. Primary eclipses allow us to estimate the extent of a spherically symmetric corona on the primary G star of about $1.3R_{\odot}$, or $0.86R_{\star}$, and indicate the G star is likely brighter than the K component by a factor of 2–5. Brightness changes not attributable to eclipses appear to be dominated by stochastic variability and are generally non-repeating. X-ray and EUV light curves cannot therefore be reliably used to reconstruct the spatial distribution of emission assuming only eclipses and rotational modulation are at work. Moderate flaring is observed, where count rates increase by up to a factor of three above quiescence. Combined with older *ASCA*, *Einstein*, *EXOSAT*, *ROSAT* and *Beppo-SAX* observations, the data show that the level of quiescent coronal emission at X-ray wavelengths has remained remarkably constant over 33 years, with no sign of variation due to magnetic cycles. Variations in base level X-ray emission seen by *Chandra* over 13 years are only ∼ 10%, while variations back to pioneering *Einstein* observations in 1980 amount to a maximum of 45% and more typically about 15%.

Subject headings: stars: activity — coronae — late-type — individual: AR Lac binaries: close — X-rays: stars

1. INTRODUCTION

AR Lac is the brightest known totally eclipsing system of the RS CVn class of close binaries. RS CVn systems have orbital periods typically between 1 and 14 days, with orbital separations of only a few stellar radii (Hall 1978). Tidal viscosity tends to synchronize the stellar rotation and orbital periods, increasing the rotation rates beyond typical values for all but the youngest single late-type stars. This rapid rotation is thought to engender strong dynamo action that makes them magnetically active and thus copious sources of chromospheric and coronal emission; they are among the very brightest stellar coronal sources observed at short wavelengths with X-ray luminosities up to ten thousand times that of the typical active Sun (e.g. Walter et al. 1978; Pallavicini et al. 1981; Drake et al. 1992; Dempsey et al. 1993; Singh et al. 1996; Makarov 2003; Pandey & Singh 2012).

Only about 1% of the Sun's surface is covered by bright active region emission during solar maximum (Drake et al. 2000), so even if the entire solar surface were covered in such emission, the RS CVn systems would still be two orders of magnitude more luminous in X-rays. These higher luminosities could be achieved through higher plasma densities, larger radial extent, or a mixture of both. It seems likely that these very active coronae include a continuously flaring component (see also Guedel 1997; Drake et al. 2000). As an eclipsing RS CVn-type system, AR Lac has played a key role in attempts to understand the morphology of these very active stellar coronae.

The first clues to the spatial structure of the AR Lac coronae came from radio observations: Owen & Spangler (1977) failed to detect an eclipse in the quiescent radio emission at 4585 MHz, a result which suggested that the radio flux originates from a region that is large compared to the radii of the component stars. From radio interferometry, Trigilio et al. (2001) determined that the emission was spatially resolved and of order of the binary dimensions; slight variability outside of eclipses suggested modulation by inhomogeneous structures.

Further progress, though with partially conflicting results, was made through direct observations of the hot coronal plasma by the *Einstein* (Walter et al. 1983), *EXOSAT* (White et al. 1990; Siarkowski 1992), *ROSAT* (Ottmann et al. 1993), *ASCA* (White et al. 1994; Siarkowski et al. 1996), *EUVE* (Walter 1996; Christian et al. 1996), and *Beppo-SAX* (Rodonò et al. 1999) observatories. The lack of an obvious eclipse in the harder of two *EXOSAT* X-ray bandpasses lead White et al. (1990) to suggest the hotter and cooler plasma resides in two distinct regions, with the harder emission coming from a much larger region, comparable to the size of the stellar system. This conclusion was bolstered by a similar

EXOSAT observation showing an apparently uneclipsed hot component on the active binary TY Pyx (Culhane et al. 1990), and fitted well with both the Owen & Spangler (1977) radio result and the finding of Swank et al. (1981) that low resolution *Einstein* spectra of active stars could be adequately fitted with discrete two-temperature models containing a hard and softer component. Subsequent EUV and X-ray studies all observed distinct primary eclipses[1], supporting the view that a significant fraction of AR Lac coronal emission must arise from a relatively compact region. Detailed reviews and discussion of these different observations have been presented by Christian et al. (1996) and Rodonò et al. (1999) .

Further insights were made spectroscopically, first with *EUVE*, and then with the *Chandra* and *XMM-Newton* observatories, both of which are equipped with diffraction gratings permitting detailed high-resolution spectroscopy in the soft X-ray bandpass (e.g. Weisskopf et al. 2003; den Herder et al. 2001). Griffiths & Jordan (1998) estimated a coronal plasma density of 5×10^{11} cm^{-3} based on Fe XXI lines. Huenemoerder et al. (2003) also found tentative evidence for high plasma densities on the order of $\log n_e \sim 11$ cm^{-3} using lines from the He-like ions of O and Ne formed around 2–4 $\times 10^6$ K. This result was confirmed by Testa et al. (2004a), who found $\log n_e = 12.5 \pm 0.5$ cm^{-3} from He-like Mg formed at slightly hotter temperatures of $\sim 6 \times 10^6$ K (see also Ness et al. 2004). Testa et al. (2004a) also analysed the *Chandra* spectra of several other active binaries and found similar high densities to generally characterise the coronae of very active stars. High densities point toward compact coronae, though without further spatial diagnostics there remains a degeneracy between surface filling factor and coronal scale height.

The degeneracy was broken for two RS CVn-type binaries stars, II Peg, IM Peg, and the active M dwarf EV Lac, that were part of a larger sample whose high-resolution *Chandra* HETG spectra were analysed by Testa et al. (2004a, 2007). These stars exhibited significant resonance scattering depletion of H-like O and Ne Lyα lines. The size of coronal structures derived from the measured optical depths for all three sources is of the order of a few percent of the stellar radius at most, indicating the presence of compact, dense and very bright emitting structures.

One drawback of existing X-ray studies of AR Lac is that data generally cover only fractions of an orbit, or concentrate on one orbital period or less. It is difficult to tell from all the disparate observations what the long-term behaviour of the source is, how repeatable any eclipses are, and what emission variations are likely to be due to rotational modulation or to simple intrinsic stochastic variability.

The high elliptical orbit of the *Chandra X-ray Observatory*, combined with high spatial resolution and relatively low noise detectors, provides an advantageous viewpoint for studying the time-dependent X-ray emission of stellar coronae. During on-orbit calibration toward the end of the summer of 1999, AR Lac was favorably placed in the sky and of the right X-ray brightness to make a suitable point-source calibration target for the *Chandra* High Resolution Camera (HRC). As such, it was the first X-ray bright late-type star observed by *Chandra*, and has been observed regularly since then to monitor instrument performance. Here we present an analysis of these data that were obtained over a period of 13 years from 1999 to 2012 and represent the most extensive set of observations of the coronae of AR Lac yet undertaken.

Following a brief summary of the adopted parameters of AR Lac in §2, in §3 we describe the observational material and data reduction; §4 and §5 present an analysis and discussion of the light curves and their implication for the structure of the AR Lac coronae, as well as the coronae of similarly active stars; a summary and conclusions are presented in §7.

2. AR LAC

AR Lac lies at a distance of 42 pc (e.g. Siviero et al. 2006), has a period of 1.983 days and comprises G2 IV and K0 IV stars of approximately equal masses but unequal radii, separated by a distance of about 9.2 $R_\odot$ (Chambliss 1976; Popper & Ulrich 1977). In the optical band, the G star is completely eclipsed by the K0 subgiant.

We adopt the system parameters of Popper (1990) and the ephemeris of Siviero et al. (2006) that is based on an extensive set of optical eclipse observations. For our purposes, this ephemeris is essentially identical to that of Marino et al. (1998), that was also adopted by Rodonò et al. (1999). The relevant parameters are listed in Table 1. While Lu et al. (2012) have more recently studied the orbital period variation of AR Lac, and have produced an analytical formula for the difference between observed and predicted eclipse times ("$O-C$") relative to the ephemeris of Siviero et al. (2006), these $O-C$ corrections do not seem to match the data of Siviero et al., with values of $O-C$ close to 0.1 days for the range of epochs on which Siviero et al. base their ephemeris. We also find that the *EUVE* and *Chandra* eclipses reported here are not consistent with the Lu et al. (2012) $O-C$ values.

3. OBSERVATIONS AND LIGHT CURVES

3.1. *Chandra X-ray Photometry*

Regular *Chandra* observations of AR Lac have been performed using the High Resolution Camera imaging and spectroscopic (HRC-I, HRC-S) detectors since the initial on-orbit calibration phase in 1999. These data were obtained for the purposes of verifying the focus and imaging performance of the combined mirror and detector assembly. The HRC instrument is of microchannel plate design with sensitivity in the 0.07-10 keV range and peaking around 1 keV, and provides photon timing resolution of a few *ms* in the standard mode employed for the data presented here (and up to 16 μs in a special "timing mode" Kenter et al. 2000) that enable accurate light curves to be constructed. Since the detectors themselves have only very low energy resolution, no attempt was made to constrain or filter detected events in energy.

The AR Lac observations were aimed at different off-axis angles to obtain pointings over a range of detector locations in a coarse "raster" , with each pointing typically lasting from one to a few ks each. Each pointing has associated "start" and "stop" times separated

[1] We adopt here the usual convention for AR Lac designating the G2 IV star to be the primary.

TABLE 1
Relevant parameters of AR Lac adopted in this study (from Popper 1990)

	Primary G2 IV	Secondary K0 IV
Mass	$1.23M_\odot$	$1.27M_\odot$
Radius	$1.52R_\odot$	$2.72R_\odot$
Inclination	$i = 87$ deg	
Primary eclipse[a]	2451745.58650+1.98318608E	

[a] From Siviero et al. (2006)

by short intervals during which the detector high voltage was ramped down. The observations are summarised in Table 2, though details of the individual pointings within each visit are omitted. In a small handful of cases, individual pointings were found to have dithered onto the High Energy Suppression Filter attached to the HRC-S and were discarded.

Satellite telemetry was processed by standard *Chandra X-ray Center* (CXC) pipeline procedures to produce photon event lists. Raw instrument count rates were examined to ensure that the data were not affected by telemetry saturation, which can lead to significant deadtime. Times of telemetry saturation and where the instrument dead time might be significant (as judged by the flag DTF< 0.98) were discarded.

Data analysis employed standard CIAO v4.5 procedures and calibration database CALDB v4.5.5. The event files were partitioned into 400 second bins (and whatever exposure remained in the final bin). For each bin, spectrum-weighted exposure maps, describing the product of effective area and exposure time, of the detector region under the dithered source region was generated using standard CIAO tools. The weighting spectrum was computed using the APEC model in XSPEC, using four discrete components normalised to match the emission measure distribution as a function of temperature of Huenemoerder et al. (2003). We emphasise that the exact choice of spectral parameters is not important here (see also Section 6). Net source counts were extracted from circular source regions whose radii depended on off-axis angle, and surrounding background annulus regions. Energy and photon fluxes were then calculated by dividing the net counts by the exposure map value in the appropriate units of the pixel at the center of the source region.

A composite of all the *Chandra* HRC-I and HRC-S observations are illustrated as a function of orbital phase in Figure 1.

3.2. *EUVE OBSERVATIONS*

AR Lac was observed with the *EUVE* Deep Survey (DS) telescope on four separate epochs, one in 1997 July, and three in 2000 September, for a total exposure time of 435 ks. Details of the observation times are listed in Table 3. Photons gathered by the DS telescope are either intercepted by three symmetrically-oriented grazing incidence diffraction gratings, or else pass through to the Deep Survey (DS) detector. On-axis photons, such as would be observed from a point source during a normal spectroscopic pointing, fall on a boron-coated Lexan filter supported on a nickel mesh, having significant transmission between approximately 65 and 190 Å and peaking near 90 Å with an effective area of about 28 cm^2. A complete description of the EUVE instrument and its performance can be found in Welsh et al. (1989) and Bowyer & Malina (1991). The sensitivity of the *EUVE* instruments in terms of optically-thin plasma emission, as is expected to characterize the coronae of active stars like AR Lac, has been thoroughly discussed by Drake (1999).

We obtained DS QPOE (quick position-ordered event) files from the *EUVE* archive and processed the data using the most current telescope effective area, vignetting corrections and "Primbsh" corrections for when the telemetry was busy. We obtained the DS light curve using the standard *EUVE* IRAF software. Light curves for the separate EUVE observations binned at 1000 s intervals are illustrated in Figure 2. A flare amounting to a peak count rate of ten times the quiescent value was detected in the last observational segment; this is illustrated in Figure 3. The data are illustrated as a function of orbital phase in Figure 4.

4. LIGHT CURVE ANALYSIS

Both *Chandra* and *EUVE* sets of light curves are characterized by stochastic variability and flaring, but also by prominent primary eclipses in the the majority of epochs in which the eclipse was covered. There are no obvious signs of the secondary eclipse in either the X-ray or EUV data; we will return to this in the discussion below.

4.1. *Constraining the coronal scale height*

The simplest coronal model to consider is a spherically-symmetric shell of emission surrounding both stars that is constant in time. Such a model has a well-behaved, symmetrical primary eclipse whose width and depth depends on the relative brightness of the two stars and the coronal scale height. Unfortunately, Figure 8 demonstrates that "clean" and perfectly symmetrical coronal primary eclipses that can easily be interpreted in terms of spherical emitting geometry are fairly rare. However, there are a number of primary eclipses in which ingress or egress does appear to follow the shape expected for such a spherical shell of emission and that are unaffected by significant flares. We have extracted these and have fitted a coronal emission model.

Our model comprises a numerical spherically-symmetric intensity profile exponentially decaying with height placed on each star. These intensity profiles are placed in a 3D cartesian system and the intensities are projected onto a plane perpendicular to the direction of observation. The disks of the stars are opaque, and the atmospheres are assumed to be fully transparent such that neither primary nor secondary corona contributes to any dimming of the corona behind it. Using the system parameters listed in Table 1, we compute the projected coronal emission as a function of orbital phase and produce artificial light curves. There are three free parameters: the K star is characterized by a scale height h_K and relative brightness b_K, and the secondary G star has a scale height h_G and a fixed brightness $b_G = 1$. The overall normalization of the model is set separately for each dataset to be the median count rate of all rates for a given instrument over the phase range $0.15 : 0.85$.

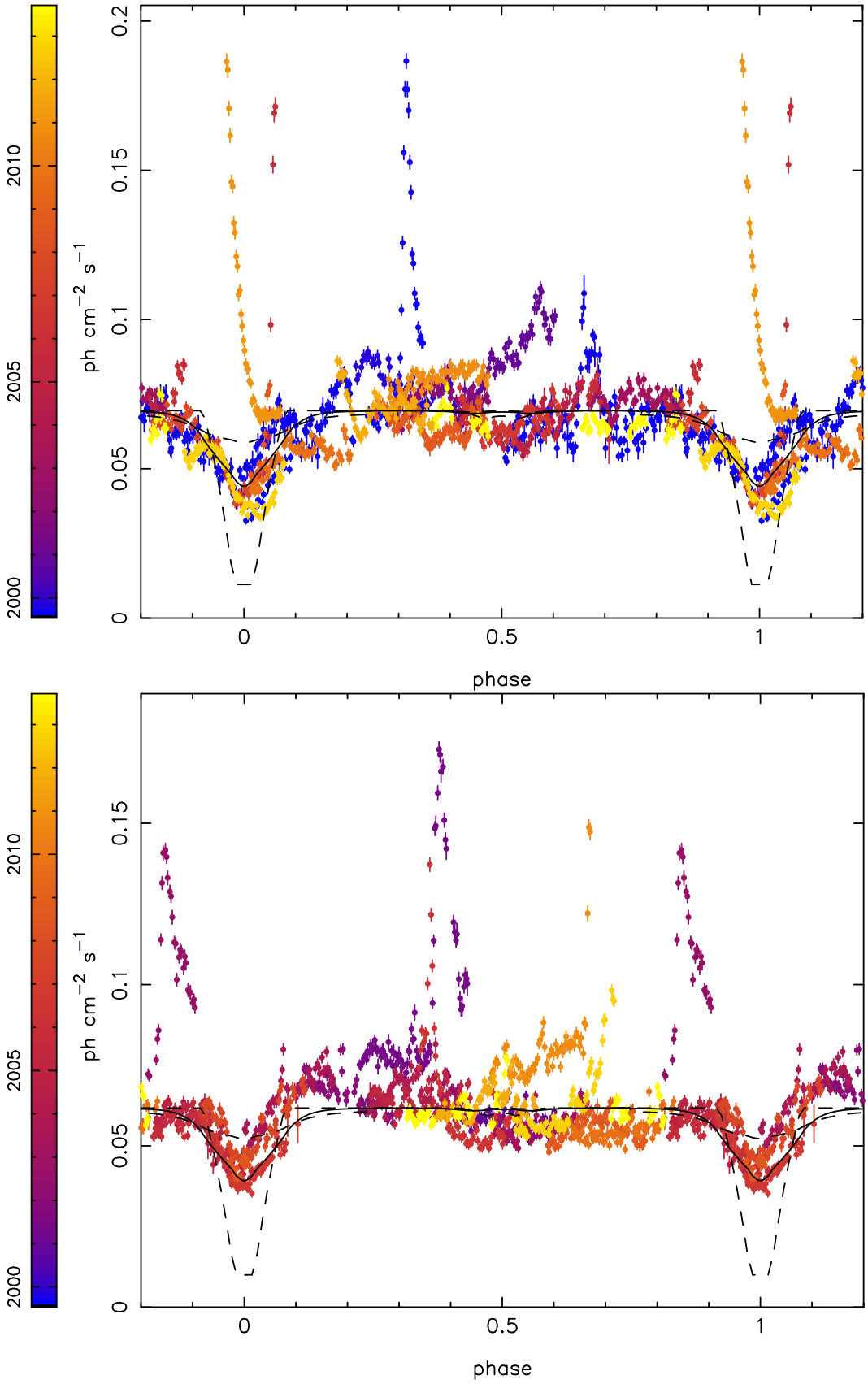

FIG. 1.— Phased composite HRC-I (top) and HRC-S (bottom) X-ray light curves of AR Lac for all the epochs listed in Table 2. Data are colour-coded according to the time of acquisition and are compared with model light curves for spherically-symmetric coronae on both components. Models, from top to bottom, are for coronal scale heights of 0.2, 0.5 and 1.0 $R_{\odot}$.

TABLE 2
Chandra HRC Observations of AR Lac used in this Analysis

Observation ID	Detector	UT First Start	UT Last Stop	Elapsed (ks)	Exposure (ks)
1283-1289, 1294-1295	I	1999-08-31T19:31:51	1999-09-01T00:41:32	19	7
1319-1382, 1385	I	1999-10-03T13:10:26	1999-10-05T05:34:48	145	103
1484-1504	I	1999-12-09T09:41:42	1999-12-09T20:40:04	40	25
996, 2345-2364	I	2000-12-12T16:31:38	2000-12-13T01:37:11	33	25
998, 2366-2385	S	2000-12-20T14:52:41	2000-12-20T23:51:27	32	24
997, 2432-2451	S	2001-05-14T00:05:25	2001-05-14T10:30:09	37	28
2625-2645	S	2002-01-26T14:09:49	2002-01-26T23:03:17	32	24
2604-2624	I	2002-01-26T23:03:17	2002-01-27T08:01:37	32	25
2646-2666	S	2002-08-09T11:30:11	2002-08-10T12:52:59	91	18
4332-4352	S	2003-02-22T00:26:08	2003-02-22T09:26:05	32	24
4290-4310	I	2003-02-22T09:26:05	2003-02-22T18:23:36	32	24
4311-4331	S	2003-09-01T09:42:51	2003-09-01T18:59:46	33	23
5081-5101	S	2004-02-09T12:59:22	2004-02-09T21:39:16	31	22
5060-5062	I	2004-09-13T20:19:58	2004-09-13T21:39:48	5	3
5063-5080, 6133-6135	I	2004-11-25T13:40:27	2004-11-25T22:21:40	31	22
5102-5122	S	2004-11-28T05:42:35	2004-11-28T14:13:21	31	22
6021-6041	S	2005-02-10T10:38:01	2005-02-10T20:24:24	35	26
6000-6020	S	2005-09-01T20:58:49	2005-09-02T06:40:12	35	26
5979-5989	I	2005-09-27T08:06:24	2005-09-27T13:38:26	20	7
5996-5997	I	2005-10-02T19:10:59	2005-10-02T20:12:35	4	2
5990-5992	I	2005-10-09T14:54:37	2005-10-09T16:47:07	7	2
5993-5995, 5998-5999	I	2005-10-17T18:19:18	2005-10-17T23:35:24	19	6
6477-6497	S	2006-03-20T05:05:39	2006-03-20T15:02:41	36	26
6519-6539	I	2006-09-20T19:20:57	2006-09-21T05:06:40	35	27
6498-6518	S	2006-09-21T18:56:18	2006-09-22T04:51:09	36	26
8298-8318	I	2007-09-17T13:08:38	2007-09-17T22:40:41	34	27
8320-8340	S	2007-09-21T17:06:23	2007-09-22T03:05:09	36	26
9682-9683	S	2008-07-11T07:47:29	2008-07-11T09:55:09	8	6
9684-9685	I	2008-07-11T09:55:09	2008-07-11T11:53:54	7	6
9661-9681	S	2008-09-02T02:37:56	2008-09-02T13:31:27	39	30
9640-9660	I	2008-09-07T09:35:46	2008-09-07T20:03:22	38	30
10578-10598	I	2009-09-24T16:07:52	2009-09-25T01:53:30	35	26
10601-10621	S	2009-09-25T21:51:14	2009-09-26T07:35:29	35	27
11889-11909	I	2010-09-25T02:40:08	2010-09-25T12:09:40	34	27
11910-11930	S	2010-09-25T12:09:40	2010-09-25T21:42:13	34	26
13182	I	2010-12-16T18:45:33	2010-12-17T00:14:08	20	18
13265, 13048-13067	I	2011-09-18T20:48:16	2011-09-19T06:06:52	34	26
13068-13088	S	2011-09-19T06:06:52	2011-09-19T15:49:50	35	26
14278-14298	S	2012-09-24T09:42:17	2012-09-24T19:23:23	35	26
14299-14319	I	2012-09-27T02:28:47	2012-09-27T12:14:25	35	27
15409-15429	I	2013-09-16T15:20:29	2013-09-18T06:39:54	142	27
15430-15450	S	2013-09-16T18:11:51	2013-09-18T08:31:45	138	26

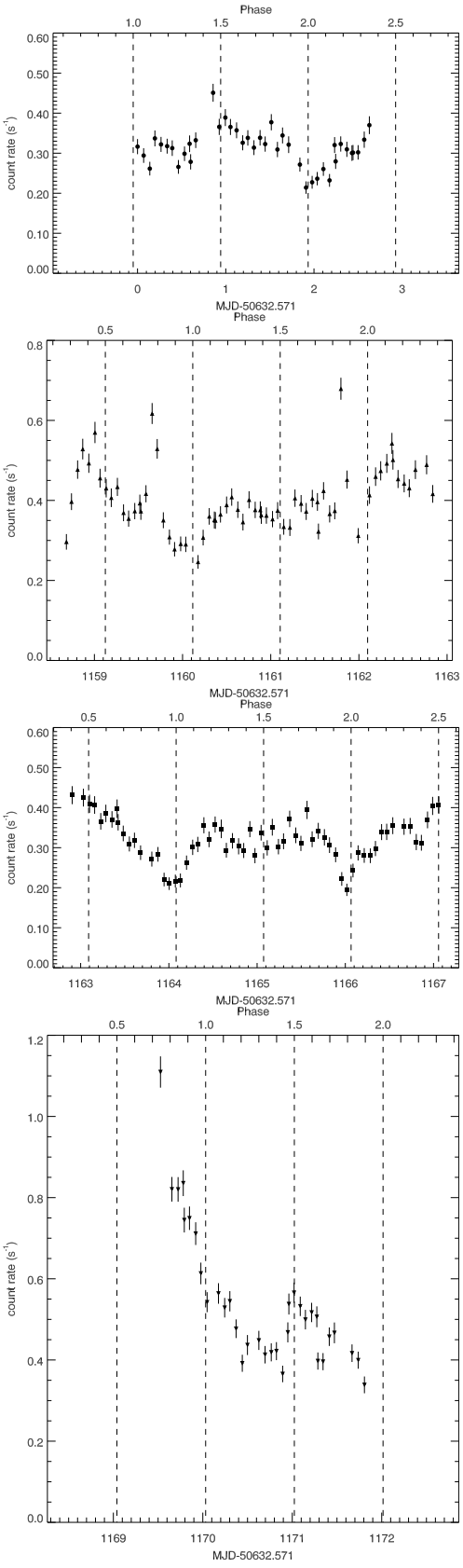

FIG. 2.— *EUVE* light curves for the four epochs analysed here. Data are binned on 1000 s intervals. Each panel is sized such that the y-axis scale is the same for all and the bottom panel does not include the flare peak at about 4.6 count s^{-1}; see Figure 3 for the full detail.

TABLE 3
EUVE OBSERVATIONS OF AR LAC ANALYSED HERE

UT Start	UT Stop	Exposure (s)
1997-07-03 13:40:17	1997-07-06 06:25:48	84758
2000-09-04 05:46:34	2000-09-08 10:12:25	137359
2000-09-08 11:08:44	2000-09-12 15:31:02	132807
2000-09-14 16:47:33	2000-09-18 00:56:34	79949

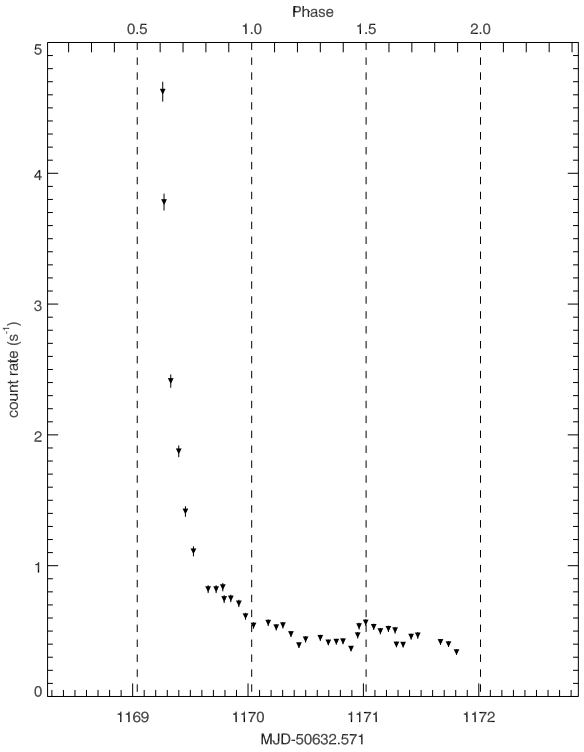

FIG. 3.— Detail of the flare detected by EUVE on 2000 September 14.

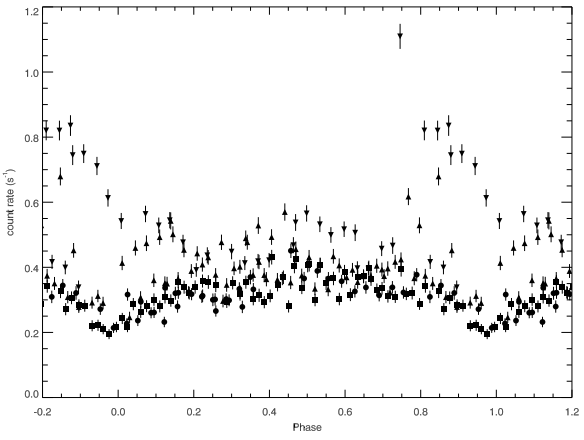

FIG. 4.— *EUVE* light curves for all four epochs shown as a function of orbital phase. Plot symbols correspond to those in Figure 2 for the four epochs analysed here. Data are binned on 1000 s intervals.

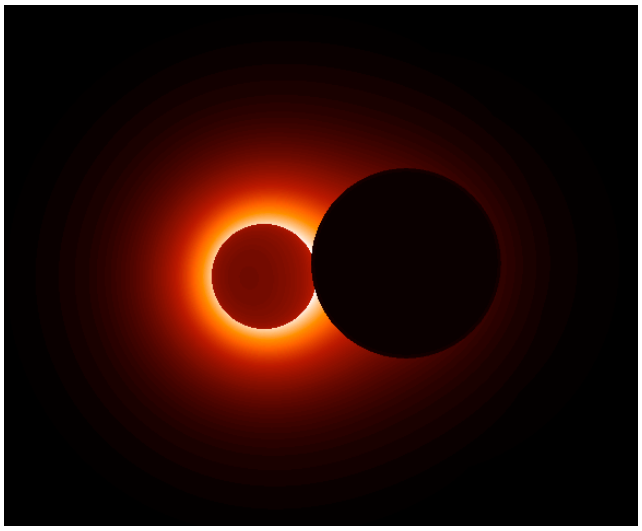

FIG. 5.— Illustration of the spherically-symmetric coronal model as the stars approach primary eclipse with the larger K star in front. Each star is assumed to be opaque and surrounded by a transparent spherical shell of emission with an exponential decline with height. The model shown correspond to the parameters $h_K = h_G = 1.3 R_\odot$, and $b_K = 0.44$.

These values were found to be 0.074, 0.064, and 0.33 ph s^{-1} cm^{-2} for *Chandra*/HRC-I, *Chandra*/HRC-S, and EUVE/DS respectively. An image of illustrating the modelling approach for typical parameters for AR Lac are illustrated in Figure 5 and illustrative model curves for different parameter values are shown in Figure 6.

Figure 6 illustrates the comparative lack of sensitivity of the eclipses to the scale height of the corona of the larger K star, h_K, even for the case in which this component is brighter than the G star. The secondary eclipse depth, when the G star is in front, changes by only 10% or so for K star scale height changes of a factor of 10 or more. We fail to detect the secondary eclipse unambiguously in any of our observations, and therefore concentrate on the analysis of primary eclipse and the G star coronal scale height.

We performed a brute-force grid search of the model parameters for the best-fit to the observations over phases ±0.15 around the primary eclipse with the K star in front. This was done for the different cases of HRC-I, HRC-S and *EUVE* data treated both separately, and with all data combined. For the combined data, fitting was also performed for ingress and egress separately. The χ^2 values are calculated assuming both a statistical error ($\propto\sqrt{\text{counts}}$ and a nominal 10% excess error attributable to intrinsic variability. The likelihood of seeing the observed data, D, given the model is then computed as $p(D|h_K, h_G, b_K) = e^{-\chi(h_K,h_G,b_K)^2/2}$. We adopt flat priors on all parameters over the grid range, and multiply them with the likelihood. Following Bayes' Theorem, this generates the joint posterior probability density distribution of the parameters given the data,

$$p(h_K, h_G, b_K|D) \propto p(h_K)p(h_G)p(b_K)p(D|h_K, h_G, b_K) \quad (1)$$

We then obtain posterior density distributions for each parameter by marginalizing over the other two,

$$p(h_K|D) \propto \int d\,h_G d\,b_K p(h_K, h_G, b_K|D) \quad (2)$$

$$p(h_G|D) \propto \int d\,h_K d\,b_K p(h_K, h_G, b_K|D) \quad (3)$$

$$p(b_K|D) \propto \int d\,h_K d\,h_G p(h_K, h_G, b_K|D), \quad (4)$$

although in practice we have no information to usefully constrain the scale height of the K star corona, h_K. The modes of the distribution correspond to locations of minimum χ^2. These, and the 68% half-tail credible regions are reported in Table 4. The model curves for the best-fit values obtained by jointly fitting all datasets (excluding periods of obvious flares) are shown in Figure 7.

The best-fit model parameters generally indicate that the G star corona has a scale height of about 1.3 solar radii and is brighter than that of the K star by a factor of 2–5. The fit parameters for HRC-I and *EUVE* are reasonably consistent with one another, while the best-fit HRC-S scale height is a factor of two smaller and the relative brightness parameter, $b_K \sim 1$, suggests both stars are of approximately equal brightness. However, visual inspection of the data and models in Figure 7 reveal substantial deviations between them, particularly at egress. This will be discussed further in Sect. 5 below.

The results for ingress and egress treated separately are generally consistent for the values of coronal scale height, within the uncertainties of the measurements. The relative brightness parameter is marginally different though, with a best-fit value slightly larger by about 40% for ingress than egress.

4.2. *Flares*

Both *Chandra* and *EUVE* observations are characterized by a number of flares. The *Chandra* flares could all be described as fairly modest, with the largest having peaks only a factor of 3 or so higher than the quiescent level, and decay timescales of a few ks. A full analysis of this flaring component is beyond the scope of this paper. The last *EUVE* epoch that began on 2000 September 14, however, happened upon a large event whose rise phase occurred before the observation start, but whose decay was tracked over two days (see Figure 3. The spectrum of the event was previously analyzed by Sanz-Forcada et al. (2003) who reported a flare fluence of 2.0×10^{35} ergs.

To refine the flare characteristics, we fitted the *EUVE* lightcurve of this large flare using Weibull distributions following the method described in detail by Huenemoerder et al. (2010). This normalized distribution is defined by the equations

$$f(p, a, s) = \left(\frac{a}{s}\right) p^{(a-1)} e^{-p^a} \quad (5)$$

$$p = (t - t_0)/s \quad (6)$$

where a is a shape parameter and takes values $a > 0$, s describes the scale or width of the distribution and is also positive, $s > 0$, and t is the time coordinate with the time of flare onset given by t_0. An amplitude parameter normalizes to the total counts, and we included a constant term as an estimate of the quiescent rate. While

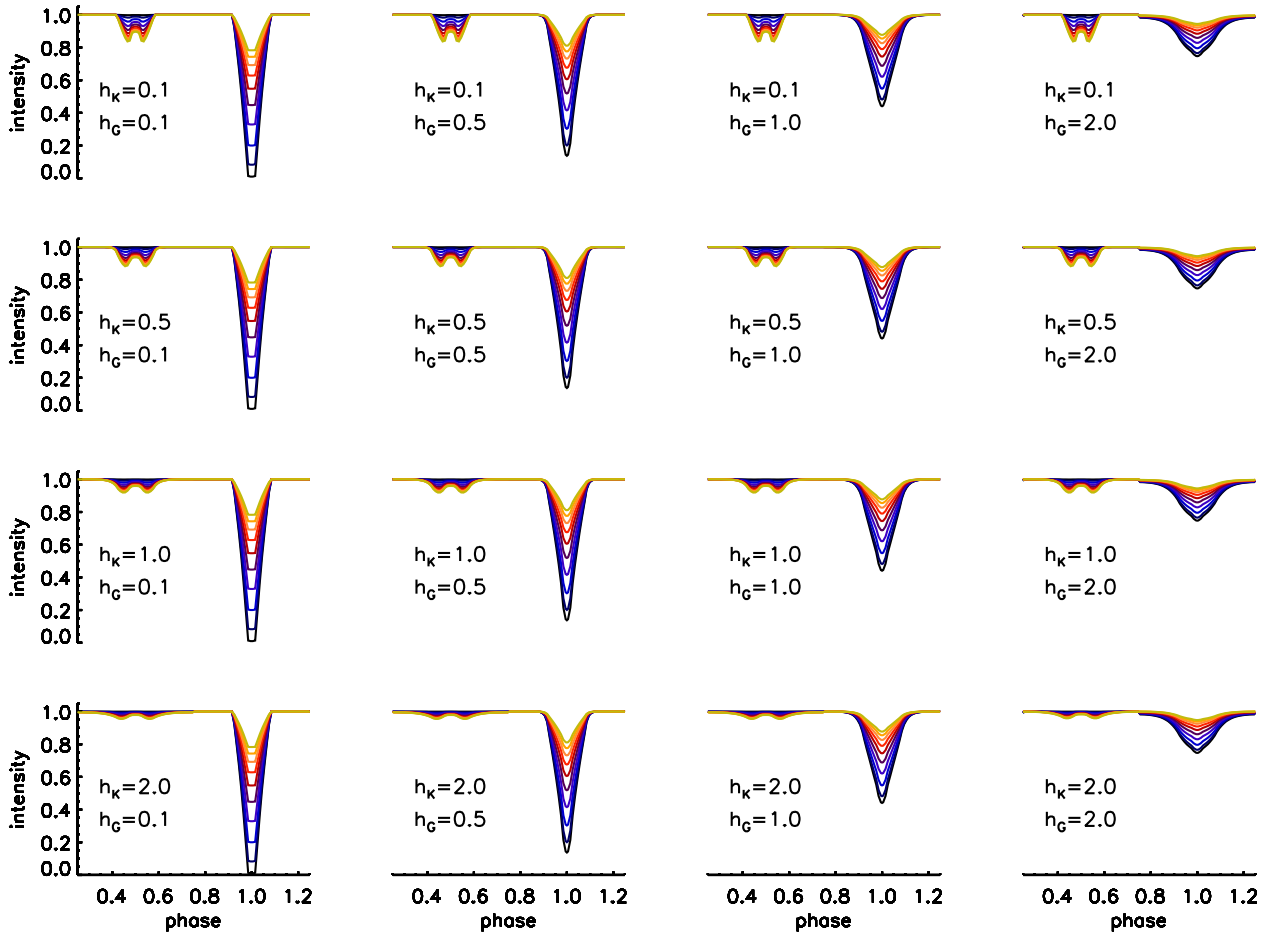

FIG. 6.— Illustration of how the primary and secondary eclipse profiles change with the free parameters in the light curve model: b_K, h_K and h_G; b_G is normalized to 1 for all models. The parameter h_K increases from top to bottom and is fixed from left to right. Conversely, h_G increases from left to right and is held fixed from top to bottom. The measure of the relative brightness of the primary and secondary coronae, b_K (with b_G being normalised to 1), goes from 0.1 (blue; dark) to 2.0 (yellow; light) in steps of 0.3.

TABLE 4
MODEL PARAMETER ESTIMATES

Dataset		h_G [$R_\odot$]	b_K	χ^2/ν
Full eclipse	HRC-I	$1.3^{<1.33}_{>1.27}$	$0.20^{<0.22}_{>0.20}$	571/389
Full eclipse	HRC-S	$0.7^{<0.74}_{>0.68}$	$1.16^{<1.16}_{>1.15}$	344/330
Full eclipse	EUVE	$1.5^{<1.59}_{>1.46}$	$0.20^{<0.3}_{>0.2}$	79/80
Full eclipse	EUVE+HRC-I+HRC-S	$1.3^{<1.36}_{>1.27}$	$0.44^{<0.48}_{>0.40}$	1357/802
Ingress	EUVE+HRC-I+HRC-S	$1.25^{<1.33}_{>1.20}$	$0.53^{<0.60}_{>0.49}$	352/358
Egress	EUVE+HRC-I+HRC-S	$1.4^{<1.44}_{>1.36}$	$0.29^{<0.38}_{>0.26}$	998/366

this is an empirical parameterization of a flare, the function can range from purely exponential form for $a = 1$, to steeper for $a < 1$, or shallower for $a >$, to smooth rise and decay for large a.

We fitted both the large flare, and a smaller event that occurred nearly two days after the observation start. The free parameters in the model are the normalization factor, a, s, and t_0 and the best-fit is illustrated in Figure 9. The large flare contains 66000 counts, a scale of 25 ks, and is slightly steeper than exponential ($a = 0.82$), while there are 4700 counts in the smaller flare, offset by 146 ks, the same scale, but slightly slower than exponential ($a = 1.2$). The constant term had a value of $0.37\,\mathrm{counts\,s^{-1}}$.

To estimate the flare energy, we used two methods. First, the scaling relations between observed counts and source flux for an isothermal spectrum with a flare-like temperature of 2×10^7 K given by Drake (1999, Table 8) indicate that one count in the *EUVE* DS Lex/B filter corresponds to an energy of about $3 \times 10^{-11}(2\pi D^2)$ erg, in the 65–195 Å bandpass, for a distance D. Here, we used an interstellar absorption column density of $N_\mathrm{H} = 2 \times 10^{18}\,\mathrm{cm^{-2}}$ derived by Walter (1996) based on *EUVE*

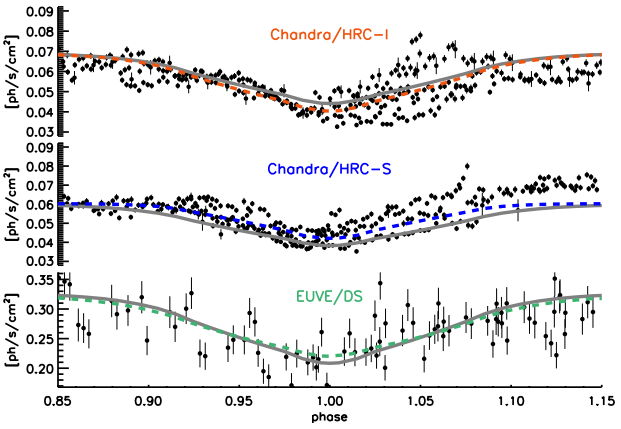

FIG. 7.— Illustration of the best-fit light curve model overlaid with the *Chandra* HRC and *EUVE* data as a function of orbital phase. Best-fits to all the data combined (grey) and to the individual data sets (colored) are shown. The best-fit parameters are listed in Table 4.

spectra of AR Lac, which is similar to the value derived by Sanz-Forcada et al. (2003). Since a flare is thought to arise on a fairly discrete, limited part of the corona, we have also divided the flux from Drake (1999) by two to remove the correction factor introduced to account for the "unseen" corona on the far side of the star (see, e.g., Jordan et al. 1987). For a total of 66000 counts, we find an EUV fluence of 2.1×10^{35} erg.

Secondly, we adopted the plasma model (emission measure distribution (EMD) and elemental abundances) of Huenemoerder et al. (2003) derived from HETG spectra obtained around the same time as the *EUVE* data, between 2000 September 11–19. However, we found their normalization too high, and had to rescale the model to an integrated emission measure of $4.9 \times 10^{53}\,\mathrm{cm}^{-3}$ to better match the X-ray spectrum of the approximately steady flux of Chandra Observation ID 9. This EMD also closely matches that derived by Sanz-Forcada et al. (2003) from the *EUVE* flare spectrum. As such, it represents some mean of flare and quiescent plasma EMDs.

For this model and a distance of 42 pc, the EUV flare photons (in the range of 65–190 Å) represent a fluence of 1.8×10^{35} ergs (a lower limit since the flare onset was not observed), in good agreement with both Sanz-Forcada et al. (2003) and the estimate based on the Drake (1999) tables. Scaling this to the HETG band (1.7–25 Å) would produce an X-ray flare fluence of 1.3×10^{36} ergs, indicating that the radiative output of the hot flare plasma is dominated by X-ray emission.

While the flare looks very large in the EUV, the estimated X-ray flare fluence is typical for large flares of young active stars, which have a similar activity level as RS CVn binaries (see, e.g. Schulz et al. 2006, figure 7).

5. DISCUSSION

Eclipse observations provide potentially powerful diagnostics of the geometry of the emitting regions and have provided the main motivation for studies of the outer atmospheres and coronae of the AR Lac system. Figures 1 and 4, however, starkly illustrate the difficulties in interpreting such data in terms of obscuration and rotational modulation. The X-ray and EUV source flux is in a

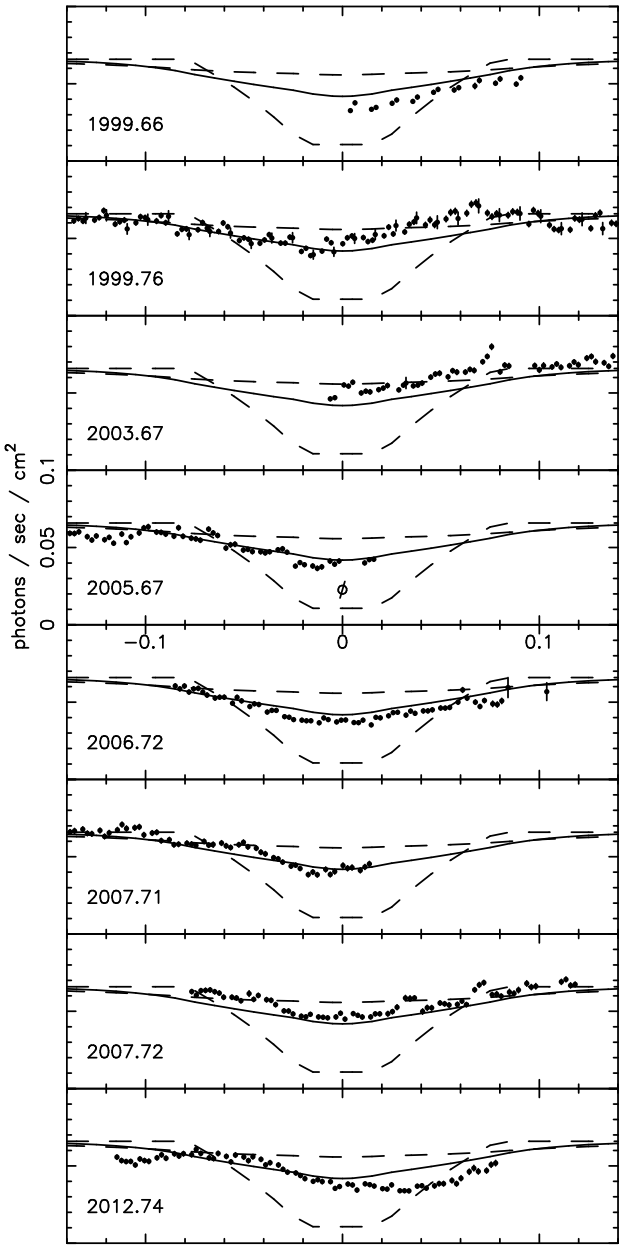

FIG. 8.— *Chandra* HRC X-ray light curves of AR Lac for data during primary eclipse that are uncontaminated by obvious flaring. Model light curves for our "best-fit" model are also shown ($h_K = h_G = 1.3R_\odot$, $b_K = 0.44$; see Table 4 for a full summary of fit results), together with those for secondary coronal scale heights of $h_k = h_G = 0$ (the deep dashed profile) and $h_K = h_G = 2.5R_\odot$ (the shallow dashed profile).

state of frequent change on a variety of timescales, and it is often unclear whether these variations are due to geometrical effects or simply reflect stochastic brightening and dimming of the emitting regions. Clear rotationally-modulated variations in coronal EUV and X-ray emission of active stars have often been sought after and occasionally seen but are not common and even when identified tend to account only for a fraction of the observed variations (see, e.g. Agrawal & Vaidya 1988; Drake et al. 1994; Guedel et al. 1995a,b; Kuerster et al. 1997; Audard et al. 2001; García-Alvarez et al. 2003; Marino et al. 2003; Flac-

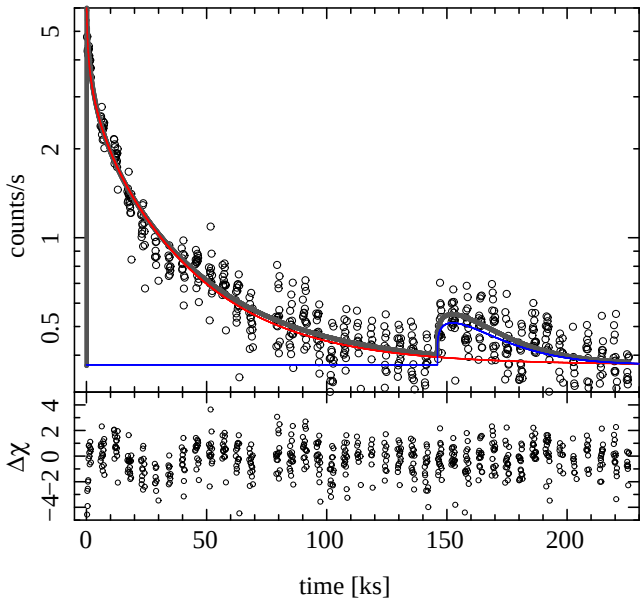

FIG. 9.— *EUVE* DS light curve, binned on 100s intervals, and best-fit Weibull distribution model and residuals for the large flare of 2000 September 14–18. The grey curve represents the overall model, while the red and blue curves illustrate the models for the large and smaller flared, respectively.

comio et al. 2005). Attempts at geometrical reconstruction of the emitting regions based on limited coverage, or only a single rotation phase, in which all variations are assumed to arise from rotational modulation, are then very likely to result in spurious structure.

5.1. *Coronal scale height and substructure*

The light curve modelling described in Sect. 4.1 at face value succeeded in constraining the coronal scale height of the G-type primary but not that of the K-type secondary star. There are three issues to consider in interpreting the results. Firstly, while it appears that simple, spherically-symmetric models with only 3 free parameters are capable of providing a reasonably good match to the observed light curves, a quasi-infinite range of models of increased complexity and asymmetry could be constructed that could match the observations equally well (or hopefully better, given more free parameters). Secondly, the observed eclipses do not all have the same profile, and can differ quite significantly between epochs. This is evident from the *EUVE* phased light curve illustrated in Figure 4, but is graphically illustrated in Figure 8, showing sequentially the *Chandra* eclipses that are unaffected by flaring. While some portions of the data follow the best-fit eclipse model quite well, such as epochs 2005.67 and the first half of the eclipse of epoch 1999.76, this is the exception rather than the norm. Thirdly, the model assumes that the emission is effectively constant throughout the eclipse, an assumption that is rendered catastrophically inappropriate during flares, but that also might be questioned during relative quiescence. We can assess the latter to some extent by examination of the light curves out of eclipse near quadrature phases, when only rotational modulation is otherwise at work.

The *EUVE* observations covering more than one orbital phase in Figure 2 demonstrate that brightness as a function of orbital phase is not very repeatable. On shorter timescales, the non-flaring data are mixed in terms of variability. There are periods of stability with little variation, such as in the HRC-S data illustrated in Figure 1 between phases 0.6 and 0.9, yet there are also a lot of brightenings and dimmings at other times, such as in the HRC-I data at phases 0.1-0.4. Asymmetries in Mg II line profiles associated with active regions on the K component were detected by Pagano et al. (2001), and it is likely that some of the eclipse asymmetries and other secular variations on orbital timescales observed here are a coronal signature of analogous active regions. Pagano et al. (2001) also noted, however, that emission on the G component appeared more uniform. Small variations might also be caused by absorbing material in the line-of-sight, as suggested by Walter (1996) based on EUV observations and inferred from the UV study of Pagano et al. (2001). In the former case, Walter (1996) estimated an equivalent absorbing column, n_H, of only 10^{19} cm^{-2} would be required, which would likely not have a noticeable affect on the higher energy X-rays observed in this study.

There is a limit to how much the non-flare variations can be caused by simple rotational modulation while still providing eclipses that follow to a reasonable degree what would be expected from a spherically-distributed corona. A compact bright active region hoving into view around the limb, for example, can cause a fairly rapid brightening, but would also cause a sharp drop as it was obscured during an eclipse. It seems more likely that the most rapid variations observed are largely changes in brightness of visible regions in the coronae of the stars than rotational modulation.

By the same argument, asymmetries in the observed eclipse profiles betray either a change in brightness of the uneclipsed plasma, spatial inhomogeneity in coronal emission, optically-thick absorbing material, or a mixture of these. Based on the eclipses observed by the *Chandra* HRC, we can point to the following epochs that have essentially full eclipse coverage but asymmetric eclipse profiles: 1999.76, whose eclipse appears narrow with an early egress; 2007.72, whose eclipse also appears narrower than spherical model predictions with a late ingress; and 2012.74, whose eclipse appears broadened with egress shifted to later times.

Narrow eclipses point to less emission from the stellar limb and might be associated with intrabinary emission located between the two stars, as has been inferred is the case in previous work. Siarkowski et al. (1996) applied an iterative deconvolution technique described by Siarkowski (1992) to *ASCA* observations in 1993 June covering slightly more than one orbital cycle. Unlike the observations presented here, secondary eclipse did appear to be present in those data, and the reconstruction of Siarkowski et al. (1996) concluded that the emission was dominated by coronal structures located between the two binary stars. We again note that this reconstruction was based on only one orbital phase, however, and it is likely that the details of the deduced spatial extent of the emission are a spurious manifestation of sort of time-variable emission afflicting the *Chandra* data as discussed above. We therefore temper interpretation of this reconstruction with some degree of caution, although it is also

notable that in this case there is an element of support for the deduced intrabinary emission from optical surface features and from Mg II line profiles of enhanced Mg II emission likely associated with extended structures corotating with the K star and close to the system center-of-mass (Pagano et al. 2001).

It is likely that coronal emission is associated with surface spots found from photometric modulation. Lanza et al. (1998) found that the spatial association between photospheric spots revealed by optical photometry and chromospheric and coronal plages as detected in the UV (e.g. Pagano et al. 2001) and the intrabinary emission deduced in X-rays by Siarkowski et al. (1996) is significant for a large active region inferred around the substellar point on the secondary and is suggested also for smaller starspots on both components. The large spots on RS CVn-type binaries, including AR Lac, appear to be fairly stable, but migrate in phase over time. On AR Lac, they are only easily discernible on the larger and optically brighter K seconary star from optical photometry and have been modelled by two large spots Rodono et al. (e.g. 1986); Lanza et al. (e.g. 1998); Siviero et al. (e.g. 2006). The migration rate of the spots was found to be 0.4 period yr^{-1} for data obtained in the years 1978–1981 (Rodono et al. 1986) and 0.55 period yr^{-1} for 2000–2005. Other spot activity on top of this pattern appears to be more irregular, with Siviero et al. (2006) noting that the light curve shaped by spots does not repeat cycle after cycle. Based on this spot behaviour, we would not expect the X-ray morphology to be stable over long periods of time, and it is perhaps not surprising that we do not find evidence for the strong intrabinary emission that appeared to characterise the 1993 *ASCA* observations, especially if such emission depends on spot activity on both stars being concentrated on the opposing hemispheres.

Proceeding with the assumption that our simple three-parameter spherically-symmetric models give a reasonable average approximation to what is more likely a distribution of discrete regions of varying brightness over the stars, we find the G star coronal scale height from Sect. 4.1 to be about $1.3R_\odot$, or in terms of the G star radius, about $0.86R_\star$. This is considerably larger than the coronal scale height on the Sun, whose typical loop lengths extend to heights of $0.04 - 0.4R_\odot$ (e.g. Aschwanden 2011). This observed loop scale height also corresponds to the pressure scale height $h_\odot = 2kT_e/\mu m_H g$: for an active solar coronal temperature of typically about $T_e = 2 \times 10^6$ K and with m_H being the proton mass, $h_\odot = 0.2R_\odot$. A larger scale height for the AR Lac coronae is expected naïvely because of lower surface gravities and higher coronal temperatures. For the G primary, the surface gravity is about half the solar value, while the typical coronal temperature is $T_e \sim 10^7$ K, or five times higher than the solar corona. The scale height is then about ten times larger or $\sim 2R_\odot$. This is approximately compatible with our observations. The surface gravity of the K component is a factor of 3 lower still, and the hydrostatic scale height is about $6R_\odot$.

The coronal scale height we find from direct geometrical eclipses is considerably larger than the $0.05R_\star$ height inferred from *EUVE* spectra for "hot" loops with temperatures in excess of 10^7 K by (Griffiths 1999, see also Griffiths & Jordan 1998), and only slightly more consistent with their finding of $0.15R_\star$ for cooler loops with temperatures less than 10^7 K. Their estimates are based on energy balance models that are somewhat dependent on the adopted gas pressure. Pagano et al. (2001) found that eclipses of the K component by the G star in the light of Mg II lines were wider than the simple photospheric geometrical prediction, pointing to a significant extension of the Mg II emitting gas above the stellar surface. Our failure to detect the eclipse of the K star in X-rays points to an extended corona, as might be expected from the greater scale height, although formally we cannot provide firm observational constraints on this.

More direct measures of coronal scale height on RS CVn-type binaries are difficult to obtain. Testa et al. (2004b) used a detection of resonance scattering in lines of O VIII and Ne IX in the coronae of II Peg and IM Peg to infer small scale heights of only a few percent or less of the stellar radius. Since such scattering was not common among the spectra they investigated, it is possible that during those particular observations the visible hemisphere emission was dominated by a bright active region core. Flare scale heights based on Fe Kα photospheric fluorescence emission of $\lesssim 0.15R_\star$ ($0.5R_\odot$) on II Peg and $\lesssim 0.3R_\star$ ($4R_\odot$) on the active K giant HR 9024 by Ercolano et al. (2008) and Testa et al. (2008), respectively, are more consistent with our geometric coronal heights. Eclipsed flares have been observed twice on Algol (B8 V+K2 III), whose optical secondary is similar to the evolved components of RS CVn-type binaries. The inferred heights of flaring loops are $\lesssim 0.6R_\star$ ($2.1R_\odot$) (Schmitt & Favata 1999) and $\sim 0.1R_\star$ ($0.35R_\odot$) (Schmitt et al. 2003); see also Sanz-Forcada et al. (2007). Our inference of scale height on AR Lac is then similar to other geometrical results for similar RS CVn-like stars.

6. X-RAYS FROM AR LAC THROUGH TIME

The HRC-I and HRC-S light curves as a function of time, in units of erg cm^{-2} s^{-1}, are illustrated in Figure 10 in the context of the fluxes observed by previous X-ray missions, beginning with *Einstein* observations in 1980 June 14 about thirty three years ago. The *Chandra* data were filtered to only include data in the phase range 0.2–0.8, outside of primary eclipse, but flares have been retained. Flux levels and uncertainties for other missions are summarised in Table 5, and were based on count rates essentially determined by eye from figures in the relevant publications in which the data have appeared. These count rates were converted to flux in the 0.5–5 keV band by folding an AR Lac spectral model through the appropriate effective area curve obtained from the Portable Interactive Multi-Mission Simulator (PIMMS) database.[2] The AR Lac model was the same as that described in Section 3.1. We also performed sensitivity tests by changing the spectral model to the two-temperature best-fit model for the out of eclipse *ASCA* observations analysed by Singh et al. (1996), and by halving the abundances of metals. In all cases, the conversions from counts to flux changed by less than 10% .

The base flux level of AR Lac—ie not considering flares—has been remarkably constant over the 13 years covered by *Chandra*, and varies by only 10% or so. Look-

[2] http://heasarc.nasa.gov/docs/software/tools/pimms.html

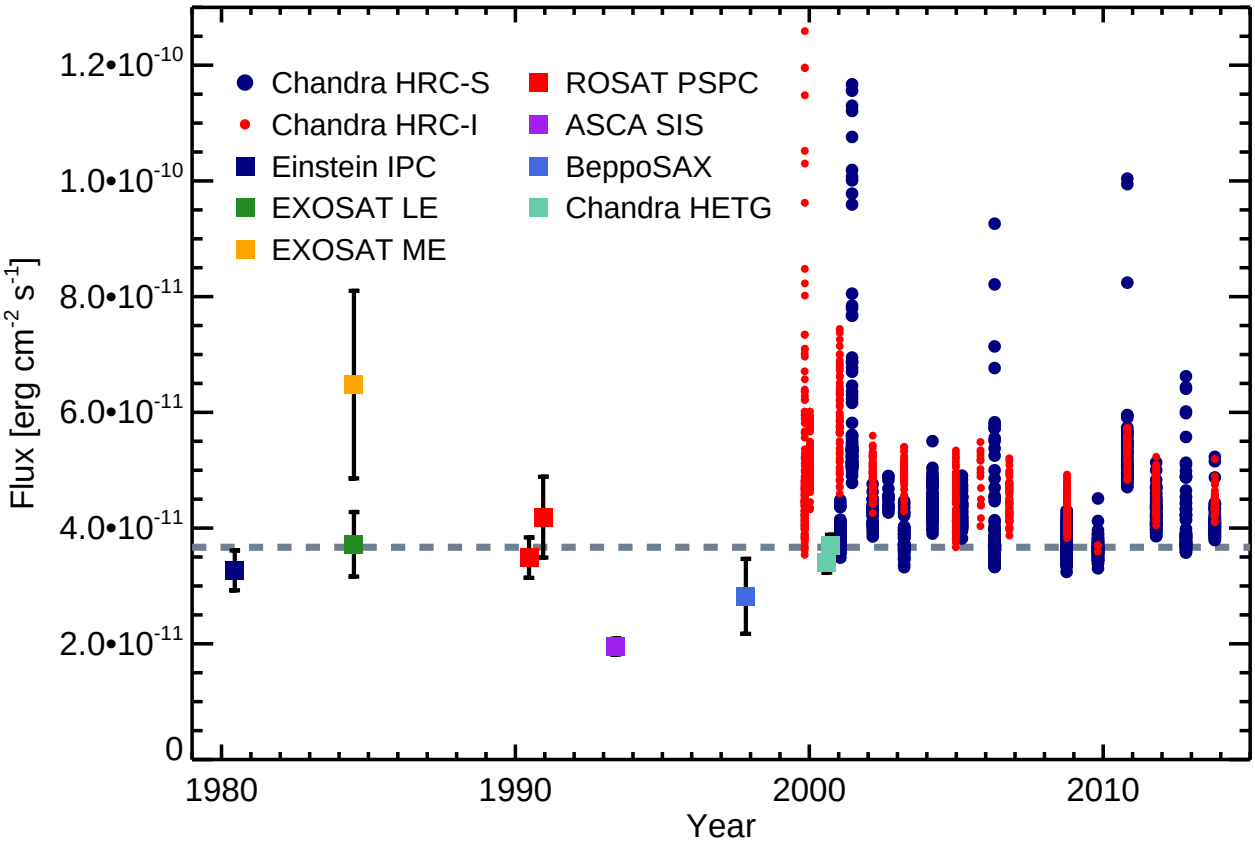

FIG. 10.— *Chandra* HRC-S and HRC-I X-ray light curves in the context of earlier X-ray observations of AR Lac. HRC data have been filtered to exclude primary eclipse within the phase range 0.8-1.2, but flares have been retained. Earlier observations are summarized in Table 5. The dashed horizontal line represents the mean of the observations prior to *Chandra*. The mean quiescent X-ray flux from AR Lac has remained consistently at 3.7×10^{-11} ergs cm^{-2} s^{-1}, to within about 10% if the *ASCA* SIS point is discarded, for the past 33 years.

TABLE 5
MULTI-DECADE OBSERVATION INFORMATION

Instrument	Date	Rate† (cts s^{-1})	Flux‡ (erg cm^{-2} s^{-1})
Einstein IPC	1980 Jun 14	1.9 ± 0.2[a]	3.2×10^{-11}
EXOSAT LE	1984 Jul 4	0.2 ± 0.02[b]	2.5×10^{-11}
EXOSAT ME	1984 Jul 4	0.5 ± 0.15[b]	2.4×10^{-11}
ROSAT PSPC	1990 Jun 18	5.0 ± 0.5[c]	3.2×10^{-11}
ROSAT PSPC	1990 Dec 11	6.0 ± 1.0[d]	3.9×10^{-11}
ASCA SIS	1993 Jun 2	1.05 ± 0.15[e]	2.0×10^{-11}
Beppo-SAX	1997 Nov 2,9	...	2.8×10^{-11}[f]
Chandra HETG	2000 Sep 11	1.0 ± 0.05[g]	3.4×10^{-11}[g]
Chandra HETG	2000 Sep 17	1.0 ± 0.05[g]	3.8×10^{-11}[g]

† Count rates listed are our own assessments of the quiescent rate outside of eclipses based on data presented in the references indicated.
‡ Except where noted, fluxes are based on the spectral model described in Sect. 3.1 and refer to the 0.5–5.0 keV bandpass.
[a] Walter et al. (1983)
[b] White et al. (1990); count rate refers to LE1 only
[c] Ottmann et al. (1993)
[d] Schmitt (1992)
[e] White et al. (1994); count rate refers to a single SIS
[f] Rodonò et al. (1999); flux taken directly from their Table 2 with uncertainty based on light curve variations in their Fig. 2.
[g] Huenemoerder et al. (2003); flux determined by direct integration of HETG spectrum

ing back further, over the 33 years of X-ray observations, the same base level is seen with only the *ASCA* observations from 1993 appearing significantly fainter than in the *Chandra* era by about 45%. The 1984 *EXOSAT* ME observation is only marginally consistent, but the instrument was only sensitive to X-ray energies above 1 keV and the derived flux is very sensitive to the adopted hot emission measure (see, e.g., White et al. 1990). The mean of the fluxes for the earlier missions, 3.7×10^{-11} erg cm^2 s^{-1}, is in good agreement with the *Chandra* measurements, while we also note that absolute calibration uncertainties of earlier missions could account for systematic differences at the 10% or so or level.

There is no evidence for any significant cyclic modulation, at least on the timescales covered by our observations. The orbital period of AR Lac has long been known to exhibit an oscillatory behaviour with a reported period of 35–50 years on top of a steady decline (Hall & Kreiner 1980; van Buren 1986; Kim 1991; Jetsu et al. 1997; Lanza et al. 1998; Qian et al. 1999; Lu et al. 2012). The origin of the oscillatory component remains uncertain though Lanza et al. (1998) noted a possible relation with a ~ 17 yr surface spot cycle attributed to the K star and suggested the period variation could be due to the Applegate (1992) mechanism that is driven by a magnetic cycle. Since the G star appears to dominate the coronal emission, its cyclic behaviour would appear to be more relevant to this study than cycles on the K star.

The long baseline of the X-ray data presented here cannot rule out magnetic cycles, but any such cycle with a period of 17 or 35 years has very little influence on the X-ray coronal energy output.

Kashyap & Drake (1999) investigated the X-ray emission of active binary stars observed at various epochs by the *Einstein* and *ROSAT* satellites and found that fluxes differed by 30–40% or so on average between different epochs. That study could only examine data averaged over whole observations, or in the case of *ROSAT*, averaged over the all-sky survey, and so any flares would be implicitly included in the averages. Figure 10 demonstrates that typical base level emission variations are likely to be significantly smaller. Relatively constant basal emission over decade timescales also appears to characterize the young K1 dwarf AB Dor Lalitha & Schmitt (2013) despite evidence for an optical cycle, and the low-mass flare star VB8 (Drake et al. 1996), and appears to be a general characteristic of very active stars.

7. SUMMARY AND CONCLUSIONS

We have analysed an extensive set of *Chandra* HRC observations of the eclipsing RS CVn-type binary AR Lac obtained over a 13 year period and combined these data with observations by *EUVE*, *ASCA*, *ROSAT*, *EXOSAT* and *Einstein* that go back to 1980. We find the quiescent base level coronal emission to be remarkably constant, with typical variations of 15% or less over a period of 33 years. Multi-orbit *Chandra* and *EUVE* observations indicate that stochastic variability likely dominates rotationally-modulated variability on orbital timescales. Consequently, reconstructions of the spatial distribution of emitting plasma should be treated with caution. Primary eclipses, when the more compact G2 IV component lies behind the K0 subgiant, are regularly detected but obvious secondary eclipses are absent. Spherically-symmetric coronal models fitted to the *Chandra* and *EUVE* light curves cannot constrain the K star coronal scale height, but indicate a coronal scale height on the G component of $1.3R_{\odot}$, or $0.86R_{\star}$, and that the G star dominates the emission by a factor of 2–5.

JJD, VK, PR and BJW were funded by NASA contract NAS8-03060 to the *Chandra X-ray Center* (CXC) and thank the CXC director, H. Tananbaum, and the CXC science team for advice and support. DPH was supported by Smithsonian Astrophysical Observatory contract SV3-73016 to MIT for Support of the Chandra X-Ray Center.

REFERENCES

Agrawal, P. C., & Vaidya, J. 1988, MNRAS, 235, 239
Applegate, J. H. 1992, ApJ, 385, 621
Aschwanden, M. J. 2011, Living Reviews in Solar Physics, 8, 5
Audard, M., Güdel, M., & Mewe, R. 2001, A&A, 365, L318
Bowyer, S., & Malina, R. F. 1991, Advances in Space Research, 11, 205
Chambliss, C. R. 1976, PASP, 88, 762
Christian, D. J., Drake, J. J., Patterer, R. J., Vedder, P. W., & Bowyer, S. 1996, AJ, 112, 751
Culhane, J. L., White, N. E., Parmar, A. N., & Shafer, R. A. 1990, MNRAS, 243, 424
Dempsey, R. C., Linsky, J. L., Schmitt, J. H. M. M., & Fleming, T. A. 1993, ApJ, 413, 333
den Herder, J. W., et al. 2001, A&A, 365, L7
Drake, J. J. 1999, ApJS, 122, 269
Drake, J. J., Brown, A., Patterer, R. J., Vedder, P. W., Bowyer, S., & Guinan, E. F. 1994, ApJ, 421, L43
Drake, J. J., Peres, G., Orlando, S., Laming, J. M., & Maggio, A. 2000, ApJ, 545, 1074
Drake, J. J., Stern, R. A., Stringfellow, G., Mathioudakis, M., Laming, J. M., & Lambert, D. L. 1996, ApJ, 469, 828
Drake, S. A., Simon, T., & Linsky, J. L. 1992, ApJS, 82, 311
Ercolano, B., Drake, J. J., Reale, F., Testa, P., & Miller, J. M. 2008, ApJ, 688, 1315
Flaccomio, E., Micela, G., Sciortino, S., Feigelson, E. D., Herbst, W., Favata, F., Harnden, Jr., F. R., & Vrtilek, S. D. 2005, ApJS, 160, 450
García-Alvarez, D., Barnes, J. R., Collier Cameron, A., Doyle, J. G., Messina, S., Lanza, A. F., & Rodonò, M. 2003, A&A, 402, 1073
Griffiths, N. W. 1999, ApJ, 518, 873
Griffiths, N. W., & Jordan, C. 1998, ApJ, 497, 883
Guedel, M. 1997, ApJ, 480, L121
Guedel, M., Schmitt, J. H. M. M., & Benz, A. O. 1995a, A&A, 293, L49
Guedel, M., Schmitt, J. H. M. M., Benz, A. O., & Elias, II, N. M. 1995b, A&A, 301, 201
Hall, D. S. 1978, AJ, 83, 1469
Hall, D. S., & Kreiner, J. M. 1980, *Acta Astron.*, 30, 387
Huenemoerder, D. P., Canizares, C. R., Drake, J. J., & Sanz-Forcada, J. 2003, ApJ, 595, 1131
Huenemoerder, D. P., Schulz, N. S., Testa, P., Drake, J. J., Osten, R. A., & Reale, F. 2010, ApJ, 723, 1558
Jetsu, L., Pagano, I., Moss, D., Rodono, M., Lanza, A. F., & Tuominen, I. 1997, A&A, 326, 698
Jordan, C., Ayres, T. R., Brown, A., Linsky, J. L., & Simon, T. 1987, MNRAS, 225, 903
Kashyap, V., & Drake, J. J. 1999, ApJ, 524, 988
Kenter, A. T., et al. 2000, in Proc. SPIE Vol. 4012, p. 467-492, X-Ray Optics, Instruments, and Missions III, Joachim E. Truemper; Bernd Aschenbach; Eds., 467–492
Kim, C.-H. 1991, AJ, 102, 1784
Kuerster, M., Schmitt, J. H. M. M., Cutispoto, G., & Dennerl, K. 1997, A&A, 320, 831
Lalitha, S., & Schmitt, J. H. M. M. 2013, A&A, 559, A119
Lanza, A. F., Catalano, S., Cutispoto, G., Pagano, I., & Rodono, M. 1998, A&A, 339, 309
Lu, Y., Xiang, F.-Y., & Shi, X.-M. 2012, PASJ, 64, 84
Makarov, V. V. 2003, AJ, 126, 1996
Marino, A., Micela, G., Peres, G., & Sciortino, S. 2003, A&A, 407, L63
Marino, G., Catalano, S., Frasca, A., & Marilli, E. 1998, Information Bulletin on Variable Stars, 4599, 1
Ness, J.-U., Güdel, M., Schmitt, J. H. M. M., Audard, M., & Telleschi, A. 2004, A&A, 427, 667
Ottmann, R., Schmitt, J. H. M. M., & Kuerster, M. 1993, ApJ, 413, 710
Owen, F. N., & Spangler, S. R. 1977, ApJ, 217, L41
Pagano, I., Rodonò, M., Linsky, J. L., Neff, J. E., Walter, F. M., Kovári, Z., & Matthews, L. D. 2001, A&A, 365, 128
Pallavicini, R., Golub, L., Rosner, R., Vaiana, G. S., Ayres, T., & Linsky, J. L. 1981, ApJ, 248, 279
Pandey, J. C., & Singh, K. P. 2012, MNRAS, 419, 1219
Popper, D. M. 1990, AJ, 100, 247
Popper, D. M., & Ulrich, R. K. 1977, ApJ, 212, L131
Qian, S.-B., Liu, Q.-Y., & Yang, Y.-L. 1999, *Chin. A&A*, 23, 317
Rodonò, M., Pagano, I., Leto, G., Walter, F., Catalano, S., Cutispoto, G., & Umana, G. 1999, A&A, 346, 811
Rodono, M., et al. 1986, A&A, 165, 135
Sanz-Forcada, J., Brickhouse, N. S., & Dupree, A. K. 2003, ApJS, 145, 147
Sanz-Forcada, J., Favata, F., & Micela, G. 2007, A&A, 466, 309
Schmitt, J. H. M. M. 1992, in Reviews in Modern Astronomy, Vol. 5, Reviews in Modern Astronomy, ed. G. Klare, 188–199
Schmitt, J. H. M. M., & Favata, F. 1999, Nature, 401, 44
Schmitt, J. H. M. M., Ness, J.-U., & Franco, G. 2003, A&A, 412, 849
Schulz, N. S., Testa, P., Huenemoerder, D. P., Ishibashi, K., & Canizares, C. R. 2006, ApJ, 653, 636
Siarkowski, M. 1992, MNRAS, 259, 453
Siarkowski, M., Pres, P., Drake, S. A., White, N. E., & Singh, K. P. 1996, ApJ, 473, 470
Singh, K. P., White, N. E., & Drake, S. A. 1996, ApJ, 456, 766
Siviero, A., Dallaporta, S., & Munari, U. 2006, Baltic Astronomy, 15, 387
Swank, J. H., Holt, S. S., White, N. E., & Becker, R. H. 1981, ApJ, 246, 208

Testa, P., Drake, J. J., Ercolano, B., Reale, F., Huenemoerder, D. P., Affer, L., Micela, G., & Garcia-Alvarez, D. 2008, ApJ, 675, L97
Testa, P., Drake, J. J., & Peres, G. 2004a, ApJ, 617, 508
Testa, P., Drake, J. J., Peres, G., & DeLuca, E. E. 2004b, ApJ, 609, L79
Testa, P., Drake, J. J., Peres, G., & Huenemoerder, D. P. 2007, ApJ, 665, 1349
Trigilio, C., Buemi, C. S., Umana, G., Rodonò, M., Leto, P., Beasley, A. J., & Pagano, I. 2001, A&A, 373, 181
van Buren, D. 1986, AJ, 92, 136
Walter, F., Charles, P., & Bowyer, S. 1978, AJ, 83, 1539
Walter, F. M. 1996, in IAU Colloq. 152: Astrophysics in the Extreme Ultraviolet, ed. S. Bowyer & R. F. Malina, 129
Walter, F. M., Gibson, D. M., & Basri, G. S. 1983, ApJ, 267, 665
Weisskopf, M. C., et al. 2003, Experimental Astronomy, 16, 1
Welsh, B. Y., Vallerga, J. V., Jelinsky, P., Vedder, P. W., Bowyer, S., & Malina, R. F. 1989, in Society of Photo-Optical Instrumentation Engineers (SPIE) Conference Series, Vol. 1160, Society of Photo-Optical Instrumentation Engineers (SPIE) Conference Series, ed. R. B. Hoover, 554–563
White, N. E., Shafer, R. A., Parmar, A. N., Horne, K., & Culhane, J. L. 1990, ApJ, 350, 776
White, N. E., et al. 1994, PASJ, 46, L97